J Nanopart Res (2011) 13:233–244
DOI 10.1007/s11051-010-0022-3

RESEARCH PAPER

Silver nanoparticles in simulated biological media: a study of aggregation, sedimentation, and dissolution

Larissa V. Stebounova · Ethan Guio · Vicki H. Grassian

Received: 22 December 2009 / Accepted: 2 July 2010 / Published online: 20 July 2010

Abstract Nanoparticles, the building blocks of many engineered nanomaterials, can make their way into the environment or into organisms, either accidentally or purposefully. The intent of this study is to provide some insight into the complex environmental, health, and safety issues associated with engineered nanomaterials. In particular, here the state of commercially manufactured silver nanoparticles—i.e., will silver nanoparticles be present as isolated particles, agglomerates, or dissolved ions—in two simulated biological media is explored. Two different commercially manufactured silver nanoparticle samples, one that has been surface modified with a thick polymer coating to render them more water-soluble and the other, with a sub-nanometer surface layer, are studied. The experimental results and the extended DLVO model calculations show that silver nanoparticles have a propensity to settle out in high ionic strength media independent of surface modification. Furthermore, single nanoparticles as well as aggregates/agglomerates are present together in these solutions. Silver ion release in these simulated biological buffers with pHs of 4.5 and 7.4 is negligible after 96 h.

Keywords Silver nanoparticles · Agglomeration · Dissolution · Sedimentation · Artificial biological fluids · Health and safety

L. V. Stebounova · V. H. Grassian (✉)
Department of Chemistry, University of Iowa, Iowa 52242, IA, USA
e-mail: vicki-grassian@uiowa.edu

L. V. Stebounova · V. H. Grassian
The Nanoscience and Nanotechnology Institute, University of Iowa, Iowa 52242, IA, USA

E. Guio · V. H. Grassian
Department of Chemical and Biochemical Engineering, University of Iowa, Iowa 52242, IA, USA

Introduction

Metal oxide and metal-based nanomaterials can be considered one of the fastest growing types of manufactured materials in the nanotechnology industry. The fate and impact of nanoparticles in aqueous environments and in the human body will depend to a large extent on the physical and chemical state of the nanoparticles. For metal and metal oxide materials, these nanoparticles can dissolve, aggregate, or remain suspended as single particles in aqueous solutions. These transitions will depend on the detailed nature of the surfaces of metal nanoparticles and the manufacture's preparation. The state of the nanoparticles, i.e., whether they are present as isolated particles, aggregate, or dissolve will also vary depending on the environmental conditions (pH, ionic strength, presence of organic matter, etc.). Thus, characterization of physical and chemical properties of nanomaterials under different conditions is essential for understanding their behavior and potential effect on the environment

and human health. Furthermore, it is important to study any toxic effects that metal nanoparticles can potentially have on biological organisms. Toxic effects can potentially be stronger for nanoscale materials since they can get into cells and deliver soluble metals or metal ions at higher rates due to their large surface area, thus causing more effective metal–bio-organisms interactions (Lok et al. 2007).

Silver nanoparticles in particular are used in many consumer products due to their antibacterial properties. Some examples of consumer products, which contain silver nanoparticles, include laundry detergents, food storage containers, textile, and shoes. The exposure to silver nanoparticles can occur from drinking contaminated water, inhalation, or through direct skin or organ contact (Luoma 2008). Therefore, silver nanoparticles can make their way into the environment or human body either accidentally or purposefully. There are only a few of in vivo toxicity studies of silver nanoparticles (Ji et al. 2007; Kim et al. 2008; Takenaka et al. 2001; Sung et al. 2008), and there are still many gaps in understanding silver nanoparticle toxicity.

Nanosilver, i.e., silver produced on the nanoscale, safety is a highly debated topic in the Environmental Protection Agency (EPA) because of its wide applications. EPA Scientific Advisory Panel released a report in January 2010 on the evaluation of the hazard and exposure associated with nanosilver and other nanometal pesticide products (SAP Minutes No. 2010-01). From this report, it was suggested that overall additional data are needed to evaluate nanosilver and its potential to induce toxicity. Thus, research in this area remains important in order to fully understand an effect of nanosilver on the human health and the environment (Damm et al. 2008; Vallopil et al. 2007; Lee et al. 2007; Ashrani et al. 2008; Wijnhoven et al. 2009). Well-designed in vitro and in vivo studies have to be performed to characterize human exposure to nanoparticles in terms of physicochemical nature, concentration, aggregation state of engineered nanomaterials (Grassian et al. 2007a, b; Pettibone et al. 2008a, b, c), and, most importantly, whether silver, in nanoparticle form, intensifies its toxic effect and poses greater risks to humans and animals.

One important step toward understanding nanomaterial behavior is to investigate the physical and chemical transformations nanoparticles undergo in aqueous environments. There are only a few studies directed toward understanding the environmental fate of nanoparticles and the potential transformation of nanoparticles in the environment (Scheckel et al. 2010; Klaine 2009; Darlington et al. 2009; Guzman et al. 2006; Lecoanet et al. 2004). From these studies, it is becoming clear that size, charge, and aggregation of nanoparticles in the transport medium are predictive of nanoparticle behavior in the environment (Darlington et al. 2009; Chen and Elimelech 2006; Vikesland et al. 2007; Skebo et al. 2007). Surface modifications, such as functionalization of the nanoparticle surface with a surfactant, for example, may reduce nanoparticle aggregation (Huang et al. 2007; Li et al. 2003). Surfactants alter nanoparticle interactions, and their presence should be taken into consideration when predicting nanoparticle behavior in the environment. Modifications to the nanoparticles size, surface, and charge either intentionally or due to the processing in the environment can influence their toxic behavior toward living organisms. Nanoparticles weakly bound together can potentially de-agglomerate and provide smaller size particles with larger surface area, which can also be excreted more easily from the body. The extent of particle aggregation can also influence their translocation to other organs. It is clear that there needs to be further systematic studies that integrate nanoparticle characterization in different environments, which includes the physical and chemical characterization of bulk and surface properties, with studies on the environmental and human health impact of manufactured nanomaterials in order to understand the molecular basis for toxicity and nanoparticle–biological interactions (Borm et al. 2006; Oberdorster et al. 2005; Powers et al. 2006).

In this study, an investigation of the fate of silver nanoparticles, including aggregation, sedimentation, and dissolution, in simulated biological fluids representative of the fluids present in the lungs is conducted to understand nanoparticles behavior once inhaled. Two different types of silver nanoparticles in two fluids, artificial interstitial fluid and artificial lysosomal fluid, are compared. The experimental data on aggregation and sedimentation is compared to the theoretical calculations based on the extended DLVO theory. This study brings insights on the processing of silver nanoparticles in high ionic fluids and demonstrates how thick polymer coatings might influence nanoparticles aggregation and dissolution. This study provides additional information on the behavior of silver nanoparticles in aqueous media.

Materials and methods

Silver nanoparticles (referred to herein as Type I Ag nanoparticles) were purchased from Nanostructured and Amorphous Materials, Inc (Houston, TX) as a powder sample. The manufacturer's specified particle diameter was given as 10 nm. Polymer-modified silver nanoparticles (referred to here as Type II Ag nanoparticles) were purchased from Vive Nano, formerly known as Northern Nanotechnologies (Toronto, Canada) in powder and suspended forms. Powder samples were resuspended in water and sonicated for at least 90 min. Resuspended samples demonstrated similar characteristics as the purchased suspensions of these nanoparticles. The manufacturer's specified particle diameter for coated Ag nanoparticles is 10 nm. Type II Ag nanoparticles were stabilized by polyacrylate sodium during the synthesis, and their surface coating consists of a polyacrylic acid polymer derivative.

Scanning mobility particle sizer (SMPS) (TSI Inc., Shoreview, MN) was used to measure particles diameters in the solutions. This method has been previously described by Elzey and Grassian (2010). In brief, SMPS spectrometer consists of three major components: an aerosol generator, a mobility classifier, and a particle counter. The electrospray aerosol generator (TSI Inc., Model 3480) produces high concentrations of monodisperse particles from 2 to 100 nm. A charged liquid solution or suspension is pushed through a capillary tube forming individual droplets. Air and CO_2 mixed with the droplets evaporate the liquid, and an ionizer neutralizes the remaining particles. Electrostatic classifier (TSI Inc., Model 3080) equipped with nano differential mobility analyzer (nano-DMA) (TSI Inc., Model 3085) is used to separate aerosols into very narrow predictable sizes based on the principle of electrical mobility. Condensation particle counter (TSI Inc., model 3775) detects airborne particles down to 2 nm. It provides highly accurate measurements over a wide concentration range from 0 to 10^7 particles/cm^3.

Transmission electron microscope (TEM) (JEOL Ltd. JEM-1230) was used to measure the primary particle sizes in dry state and monitor aggregation state of the nanoparticles exposed to different environments. Nanoparticles and agglomerates/aggregates from the solutions were deposited on TEM cooper grids using the electrospray aerosol generator (TSI Inc., Model 3480) by electrostatically driving the solution of nanoparticles through a capillary tube with a diameter of 40 μm.

Sedimentation of the nanoparticles was monitored by detecting a decrease in the intensity of the surface plasmon resonance (SPR) absorbance peak at around 400 nm using UV–Vis spectrometer (Perkin Elmer, Lambda 20). The stability of nanoparticles in different media was further determined by measuring zeta potentials of the particles using dynamic light scattering (DLS) (Malvern Instruments, Zetasizer Nano-ZS). DLS was also used to measure hydrodynamic diameter of silver nanoparticles in water.

Dissolution studies were conducted in two different types of artificial fluids using inductively coupled plasma optical emission spectrometer (ICP-OES) (Varian Inc. 720-ES). Ag nanoparticles were incubated in artificial interstitial fluid (Gamble's solution) and artificial lysosomal fluid (ALF solution) for up to 96 h at 38 °C at concentrations of 0.2–2 mg/mL. The simulated fluids were prepared using the procedures described by Stopford et al. (2003). The chemical compositions of the solutions are shown in Table 1. The smaller concentration of 0.2 mg/mL was used for

Table 1 Chemical compositions of Gamble's and ALF solutions (Stopford et al. 2003)

Artificial biological fluid	pH	Composition (per liter DI water)
Gamble's (artificial interstitial fluid)	7.4	$MgCl_2{\cdot}6H_2O$ (0.2033 g), NaCl (6.0193 g), KCl (0.2982 g), Na_2HPO_4 (0.1420 g), $NaSO_4$ (0.0710 g), $CaCl_2{\cdot}2H_2O$ (0.3676 g), $CH_3COONa{\cdot}3H_2O$ (0.9526 g), $NaHCO_3$ (2.6043 g), sodium citrate dihydrate (0.0970 g)
ALF (artificial lysosomal fluid)	4.5–5.0	NaCl (3.210 g), NaOH (6.000 g), citric acid (20.800 g), $CaCl_2$ (0.097 g), $NaH_2PO_4{\cdot}7H_2O$ (0.179 g), $NaSO_4$ (0.039 g), $MgCl_2{\cdot}6H_2O$ (0.106 g), glycerin (0.059 g), sodium citrate dehydrate (0.077 g), sodium tartrate dehydrate (0.090 g), sodium lactate (0.085 g), sodium pyruvate (0.086 g), formaldehyde (1.000 mL)

Type II Ag nanoparticles, and a larger concentration of 2 mg/mL was used for Type I Ag nanoparticles to insure that some nanoparticles remain suspended in the buffer after several days despite sedimentation. The ALF solution simulates the composition and pH of alveolar and interstitial macrophages (Stopford et al. 2003), and the Gamble's solution simulates interstitial fluid in the lungs (Moss 1979). The pH of Gamble's solution was adjusted to 7.4 by bubbling CO_2 gas through the solution, and the pH of ALF solution was 4.5 as prepared. The nanoparticles were stirred in these fluids at 38 °C. At certain periods of time about 4 mL of the nanoparticle-biological fluid solution was taken and filtered by a syringe through 0.2-μm filter and centrifuged for 30 min at 14,000 rpm in order to remove nanoparticles and aggregates that were not dissolved. The filtered and centrifuged solutions were analyzed by ICP-OES.

Results and discussion

Ag nanoparticles characterization in water

The characterization of the commercial Ag nanoparticles used in these studies was done previously (Elzey and Grassian 2010; Schmoll et al. 2009). In summary, Type I Ag nanoparticles have a thin coating on the surface detected by X-ray photoelectron spectroscopy indicating the presence of carbonate species and some carbon-oxygen functionality, likely due to the use of polyvinylpyrrolidone (PVP) during synthesis. This coating, a monolayer in thickness, accounts up to 17% of the Type I Ag nanoparticles mass, as determined by ICP analysis, which corresponds to a coating thickness of approximately 0.7 nm. The second type of Ag nanoparticles studied in this work, Type II Ag nanoparticles have a polymer coating specially synthesized to prevent the nanoparticles from aggregating. An average hydrodynamic diameter of the Type I Ag nanoparticles is in the range 11.7 ± 3.5 nm, and a hydrodynamic diameter of Type II Ag nanoparticles is 6.5 ± 2 nm as measured by DLS in water (Fig. 1). TEM imaging combined with SMPS results indicates that the primary particle diameter of Type II Ag nanoparticles is ca. 4 nm and a coating thickness is ca. 1.5 nm for a total of particle diameter of ca. 7 nm (TEM analysis is shown in Pettibone et al. 2008a and SMPS analysis is shown in Schmoll et al. 2009). This also agrees with the ICP analysis showing that there is only ca. 25% Ag by mass present in the Type II nanoparticles. For Type I Ag nanoparticles, the hydrodynamic diameter distribution is broad and suggests that some agglomerates as well as large particles are present in the water (Elzey and Grassian 2010).

Aggregation of Ag nanoparticles in simulated biological fluids

Changes in size and state of aggregation of both types of Ag nanoparticles were monitored while they were incubated in the simulated biological fluids. Figure 2a shows the diameter distribution for Type I Ag nanoparticles incubated in Gamble's solution for 72 h measured using SMPS. An average diameter of these Ag nanoparticles fluctuates between 8 and 12 nm, not showing a steady decrease which would indicate silver dissolution. A count decrease over time in Fig. 2a could indicate that some of the primary particles form aggregates that settle out of the solution. Precipitation in these solutions is also visualized. Ag nanoparticles from Gamble's solution were collected on TEM grids after their diameters were measured by the SMPS.

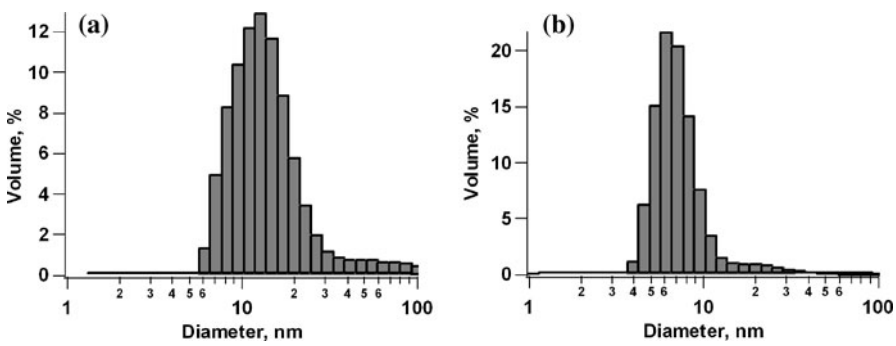

Fig. 1 Size distributions of Type I (**a**) and Type II (**b**) silver nanoparticles measured by DLS in water

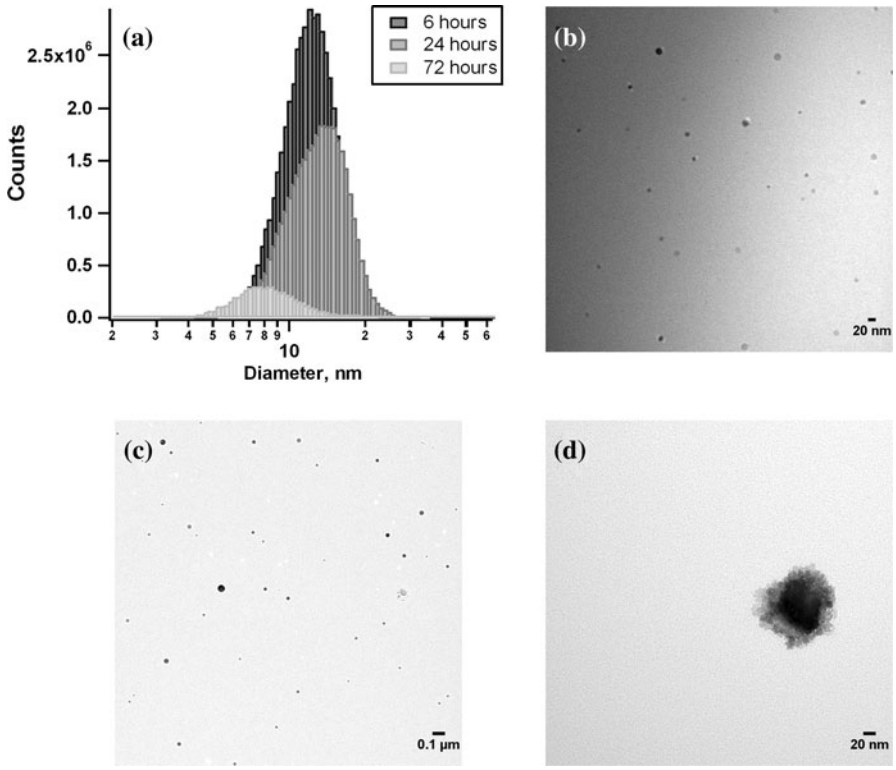

Fig. 2 **a** Diameters of Type I Ag nanoparticles at different incubation times in Gamble's solution measured by SMPS. **b–d** TEM images of Type I Ag nanoparticles deposited from Gamble's buffer at 12 (**b**), 24 (**c**), and 72 h (**d**) incubation time

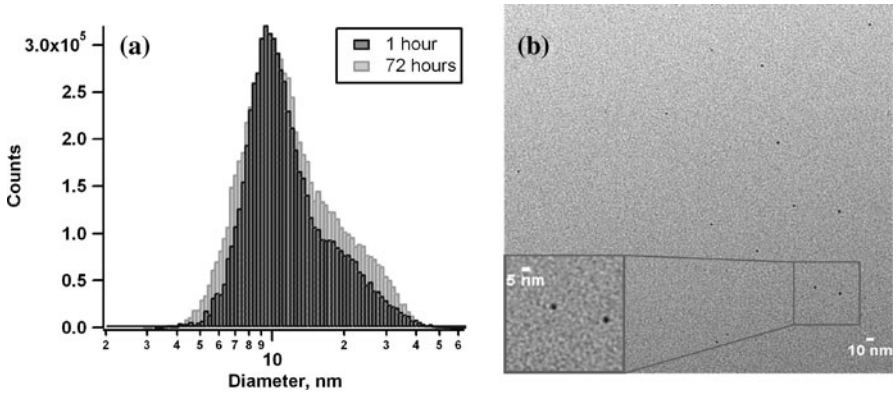

Fig. 3 **a** Diameter distributions of Type II Ag nanoparticles deposited from Gamble's solution. **b** TEM image of Type II Ag nanoparticles deposited from Gamble's solution after 12 h

Figure 2b–d shows TEM images of Type I Ag nanoparticles deposited from Gamble's solution after 6, 24, and 72 h. These results are consistent with the measurements on SMPS: particles counts decrease slightly after 24 h, and large aggregates are seen in TEM images after 72 h that cannot be detected by nano-SMPS and can thus explain the significant decrease in the number of particles.

Figure 3a shows the diameter distributions for Type II Ag nanoparticles incubated in Gamble's solution. The diameter distribution does not change significantly after 72 h, indicating that some amount of Type II Ag nanoparticles remains stable in this buffer during this period of time. The TEM image collected after 12 h of incubation of Type II Ag nanoparticles in Gamble's solution (Fig. 3b) also shows single nanoparticles with diameters of ca. 3 ± 1 nm. This is most likely representative of the silver core of the Type II Ag nanoparticles as it is difficult to detect organic coatings with TEM due to

the poor contrast. Although the particle count does not change significantly in Fig. 3a, gray-colored precipitates were visualized in Type II Ag nanoparticle solutions after a few hours. These precipitates are Ag nanoparticles that settle out. Since we probe nanoparticles from the top of the solution for the SMPS and TEM analysis, we do not account for all aggregates and agglomerates that settle out. While the result from Fig. 3a implies that all Type II Ag nanoparticles remain suspended after 72 h, these observations along with the UV–Vis measurements described below indicate that there is significant settling of the Type II Ag nanoparticles after just a few hours. SMPS equipped with a nano-DMA detects nanoparticles in the range 2–70 nm and has a high sensitivity in this size range; therefore, it is difficult to predict the amount of precipitated silver from SMPS data alone.

The dissolved and precipitated Ag nanoparticles in the biological fluid suspensions were digested separately in HNO_3. The ICP analysis of the digested solutions revealed that less than 1% of nanoparticles remains in the solution and 99% of nanoparticles settled out 24 h after the suspensions were made. This leads us to conclude that the initial concentration strongly affects the stability and sedimentation of silver nanoparticles. In the case of Ag nanoparticles protected by a polymer coating from aggregation, there is still a critical concentration above which nanoparticles destabilize and settle out. One percent of the total nanoparticle concentrations used in this study corresponds to a concentration in the range 2–20 mg/L. This conclusion agrees with observations from other reports indicating that a toxic effect of Ag nanoparticles at concentrations higher than 10 mg/L in aqueous solutions cannot be properly assessed due to aggregation and precipitation (Bastus et al. 2008). However, other reports indicate that Ag nanoparticles can be toxic to cells even at 10 mg/L (Hussain et al. 2005).

Both types of Ag nanoparticles studied here did not form stable suspensions in ALF buffer. This complicated the analysis of these solutions, especially for the solutions containing Type I Ag nanoparticles. The reason for this instability could be due to an increased ionic strength of ALF buffer compared to water and Gamble's solution. ALF solution has the largest percent by weight of citric acid to imitate protein binding and other ligands such as acetate, to represent organic acids present in lysosomal interstitial fluid (Pettibone et al. 2008b). TEM imaging of the Type II Ag nanoparticles deposited from the ALF solution after 72 h reveals large clusters with different shapes, which most likely are salt clusters crystallized in this simulated solution. We observed that ALF buffer salts also produce nanosized particles, which create a diameter distribution centered around 11 nm without any Ag nanoparticles added. Therefore, we could not dissociate between silver nanoparticles and the particles produced by the buffer salts in the SMPS distribution data. It should be noted that we did not observe any distributions in the SMPS analysis of Gamble's solution and water before an addition of Ag nanoparticles.

Sedimentation and stability of Ag nanoparticles

UV–Vis spectroscopy can be used to quantify sedimentation rate of nanoparticles in solution (Pettibone et al. 2008c). Surface plasmons produce a strong resonance peak centered between 400 and 450 nm in the absorption spectrum of Ag nanoparticles (Englebienne et al. 2003; Smitha et al. 2008; Heath 1989; Lee et al. 2008). In this study, UV–Vis spectroscopy was used to monitor changes to the SPR peak intensity as a function of time in order to measure sedimentation rate in the nanoparticles suspensions. As shown in Fig. 4a, an SPR peak is centered at 423 nm for Type II Ag nanoparticles suspended in water. The peak position shifts to $\sim$400 nm for the same nanoparticles suspended in Gamble's solution. SPR can be influenced by a number of factors, such as solvent dielectric constant, nanoparticle size, and surface functionalization (Smitha et al. 2008). Here, both the solutions and the nanoparticles can change their optical properties due to interactions which could affect the dielectric constants and shift the resonance peak position. The SPR peak almost disappears after 24 h in Gamble's buffer. This observation coincides with the discoloration of the nanoparticle suspension, and an appearance of silver precipitates. Figure 4b shows UV–Vis spectra collected from Type II Ag nanoparticles suspended in ALF simulated biological buffer. The SPR peak disappeared before 1 h; the nanoparticle solution changed its color from brown to white/transparent immediately after mixing with ALF buffer, and the precipitates appeared almost immediately. A large

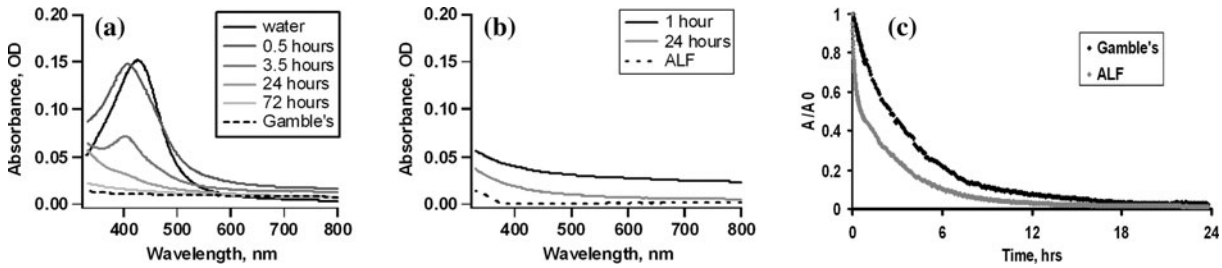

Fig. 4 UV–Vis spectra of Type II Ag nanoparticles suspended in Gamble's (**a**) and ALF (**b**) solutions. The nanoparticles aggregated and settled out very quickly in ALF buffer, thus no SPR peak was observed. **c** Sedimentation plots collected in ALF and Gamble's buffers around 400 nm for 24 h

background signal in Fig. 4b could indicate a scattering light from large agglomerates formed in the ALF solution. Some of the agglomerates settled out after 24 h; hence, smaller background signal is observed. Figure 4c shows sedimentation plots in ALF and Gamble's solutions. The nanoparticles settle out faster in ALF buffer where half of the nanoparticles settled out in less than 1 h.

The stabilities of Ag nanoparticles in the solutions were tested using DLS (Nallathamby et al. 2008). Zeta potentials of Ag nanoparticles measured in simulated biological buffers and water are shown in Table 2. The measurements were taken 1 h after the nanoparticles were added to the buffers. An increase in absolute value in zeta potential indicates an increase in the surface charge and consequently higher stability of Ag nanoparticles in the solution. As can be seen from Table 2, the nanoparticles have higher absolute value zeta potentials in water; hence, they are more stable in water than in the simulated biological fluids. And, Type II Ag nanoparticles are more stable in both biological fluids than Type I Ag nanoparticles, which do not have protective coating, due to higher surface charges. Nevertheless, zeta potential of Type II Ag nanoparticles decreases significantly in ALF buffer, which also indicates a decrease in stability.

Table 2 Zeta potentials of Ag nanoparticles suspended in different media

Buffer/sample	Water	Gamble's	ALF
Type I Ag	−33 mV	−14 mV	−5 mV
Type II Ag	−60 mV	−31 mV	−21 mV

DLVO theory

According to classic Dejaguin–Landau–Verwey–Overbeek (DLVO) theory, the stability of particles is determined by the net electrostatic surface interactions of the particles. The total interaction energy between nanoparticles consists of van der Waals attraction (Eq. 1) and electrostatic repulsion (Eq. 2) (Lee et al. 1998):

$$V_{\mathrm{vdW}} = -\frac{A}{6}k_{\mathrm{B}}T\left[\frac{2R^2}{d^2-4R^2}+\frac{2R^2}{d^2}+\ln\left(\frac{d^2-4R^2}{d^2}\right)\right] \quad (1)$$

$$V_{\mathrm{elec}} = 2\pi\varepsilon_{\mathrm{r}}\varepsilon_0\psi_0^2 R k_{\mathrm{B}}T\ln[1+\exp(-kd)] \quad (\text{in the case of } kd>5), \quad \text{where } k=\left[\frac{1000e^2N_{\mathrm{A}}(2I)}{\varepsilon_{\mathrm{r}}\varepsilon_0 k_{\mathrm{B}}T}\right]^{1/2}. \quad (2)$$

where A is a Hamaker constant, k_{B} is the Boltzmann constant, $T = 311$ K is the body temperature, R is the radius of the particles, assuming that all nanoparticles have the same radius, d is the separation distance between the particles, ε_{r} is a relative dielectric constant of the liquid, ε_0 is the permittivity of the vacuum, ψ_0 is the surface potential of the particles, k is the inverse Debye length, e is the elementary charge, N_{A} is the Avogadro number, and I is the ionic strength of the solution.

The extended DLVO theory takes into account non-electrostatic ion-specific forces (Bostrom et al. 2006). In case of the ligand-coated nanoparticles, the interactions between the solvent molecules and the ligand tails can be responsible for the steric stabilization of the nanoparticles (Shah et al. 2002). The nanoparticles can experience significant steric repulsion due to the osmotic and elastic contributions.

Osmotic contribution (Eq. 3) depends on the molecular volume of solvent v_1, volume fraction of polymer within the coating layer Φ_p, the Flory–Huggins interaction parameter χ, particle radius R, polymer layer thickness w, and the separation distance between the particles cores d (Shah et al. 2002):

$$\begin{aligned} V_{osm} &= 0 \quad 2w \le d \\ V_{osm} &= \frac{4\pi R k_B T}{v_1}\phi_p^2\left(\frac{1}{2}-\chi\right)\left(w-\frac{d}{2}\right)^2 \quad w \le d < 2w \\ V_{osm} &= \frac{4\pi R k_B T}{v_1}\phi_p^2\left(\frac{1}{2}-\chi\right)w^2\left(\frac{d}{2w}-\frac{1}{4}-\ln\left(\frac{d}{w}\right)\right) \\ & \quad d < w \end{aligned} \tag{3}$$

Elastic repulsive energy V_{elas} originates from the entropy loss that occurs upon compression of the coating layer and might give a significant contribution to the total interaction energy when the separation distance does not exceed total particle diameter (Shah et al. 2002). The total interaction energy consists of V_{vdW}, V_{elec}, V_{osm}, and V_{elas}:

$$V_{tot} = V_{vdW} + V_{elec} + V_{osm} + V_{elas} \tag{4}$$

The interaction energy between Ag nanoparticles was calculated using Eqs. 1–4. Figure 5a shows the total interaction energy calculated using classic DLVO theory for Type I Ag nanoparticles in different solvents. We used the following parameters: Hamaker constant $A = 0.997$ eV calculated for Ag–water interaction (Shah et al. 2002), particle radius $R = 5.8$ nm, dielectric constant of water $\varepsilon_r = 80.1$, zeta potentials ψ_0 were obtained using DLS in different solvents (Table 2). It was assumed that the surface potentials were the same for both particles and remained unchanged as particles approached each other. The ionic strengths $I_{Gamble's} = 175$ mol/m^3 and $I_{ALF} = 340$ mol/m^3 were calculated based on the salt concentrations provided in Table 1. The ionic strength of 1 mol/m^3 was used to represent a low ionic strength solution or water. Considering only van der Waals attractive and electrostatic repulsive forces for Type I nanoparticles in simulated biological fluids, the attraction dominates the interaction energy, and there is no energy barrier to resist aggregation (Fig. 5a). In the low ionic strength solvent, a small energy barrier ($\sim$2.7 kT) (Fig. 5a) can keep particles from immediate collapse. This is in good agreement with the faster aggregation observed experimentally in ALF and Gamble's solutions compared to water.

Figure 5b represents total interaction energy between Type II Ag nanoparticles calculated using classic DLVO theory. The particle radius used in Eqs. 1 and 2 is 2 nm, which represents the Type II Ag nanoparticle core radius. Here we observe that an energy barrier of $\sim$10 kT needs to be overcome before particles aggregate and sediment in all of the solutions studied. Classic DLVO theory does not take into account the steric interaction between the solvent molecules and polymer ligands from the nanoparticle coating. The osmotic repulsion was calculated using Eq. 3 and added to the total interaction energy of Type II Ag nanoparticles, which have polymer coating thickness comparable with the nanoparticle diameter, in Gamble's buffer and water (Fig. 5c, d, correspondingly). In our calculations we used $v_1 = 2.99 \times 10^{-29}$ m^3 as a volume of water molecule, the polymer volume fraction $\Phi_p = 0.01$, which was adapted from Phenrat et al. (2008) and the Flory–Huggins interaction parameter $\chi = 0.45$ (Phenrat et al. 2008; Shah et al. 2002). The polymer layer thickness $w = 1.5$ nm was determined experimentally using SMPS and TEM techniques. We disregarded the elastic repulsion energy that is a part of the steric interaction in these calculations because it is negligible compared to the osmotic energy at the separation distances smaller than 4 nm. In Fig. 5c we see that the osmotic repulsion dominates all the forces at distances less than $2w = 3$ nm at which the coating layers from two interacting particles are in physical contact. Once the particles loose physical contact, the electrostatic repulsion keeps them apart until the energy barrier is less than 3/2 kT, which represents the energy of the Brownian motion. As can be seen from Fig. 5c, the repulsive energy becomes smaller than the energy of the Brownian motion at the separation distances >3.5 nm in Gamble's buffer. This means that the nanoparticle suspension in the simulated biological fluid is mostly unstable. The electrostatic repulsion extends for distances up to 24 nm in the low ionic strength fluid (Fig. 5d); hence, the nanoparticle suspension is more stable. We observed experimentally that polymer-coated Type II Ag nanoparticles are stable in water, and precipitate in the simulated biological fluids after 1 h where faster sedimentation of Type II Ag nanoparticles in ALF buffer is detected. The experimental observations agree with the extended DLVO theory results.

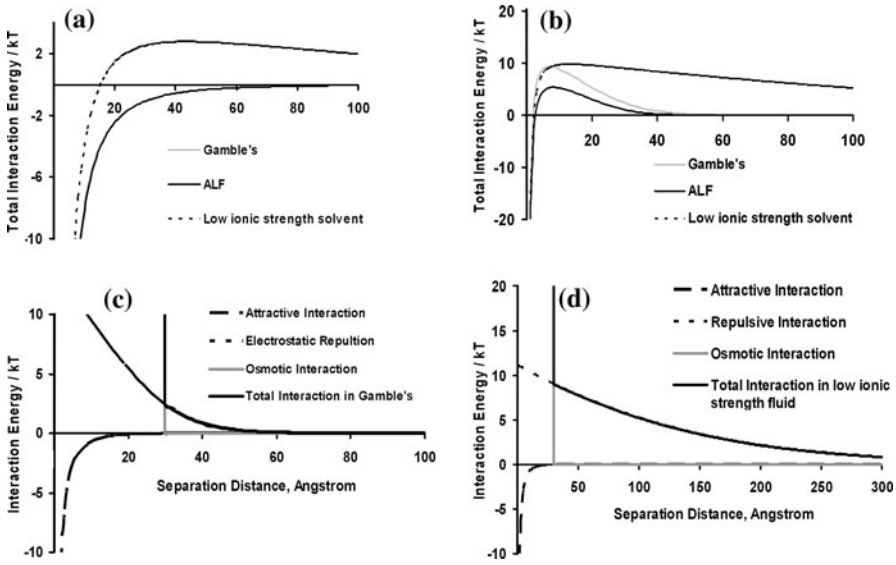

Fig. 5 Potential energy of interactions of Ag nanoparticles in different solvents. **a** Total interaction energy calculated for Type I Ag nanoparticles using classic DLVO theory. **b** Total interaction energy calculated for Type II Ag nanoparticles using classic DLVO theory. **c** Interaction energy calculated for Type II Ag nanoparticles in Gamble's using extended DLVO theory. **d** Interaction energy calculated for Type II Ag nanoparticles in low ionic strength fluid using extended DLVO theory

The DLVO calculations for Ag nanoparticles-simulated biological fluids systems described above are conducted for the non-specific polymer coating due to absence of sufficient information about the Type II Ag nanoparticle coating. For Type I Ag nanoparticles we disregarded the sub-nanometer surface layer in these calculations and assume the nanoparticles were bare for comparison to Type II Ag nanoparticles. We also did not take into account the changes in the polymer chain conformations in different solvents and interactions of the ions present in the simulated biological fluids with the nanoparticles. Moreover, it is shown that ion-specific forces (such as ionic dispersion potentials and ionic solvation energy changes) can change the nanoparticle fate in the solutions, especially at typical biological salt concentrations. Lee et al. (1998) showed that the solvation energy can make a significant contribution to the total interaction energy and the stability of the nanoparticles. Hence, the aggregation and sedimentation of nanoparticles will also depend on the type and amount of ions present in the solutions. Furthermore, the polymer coating might become unstable and dissolve in the high ionic strength fluid. This will change the chemistry of the solution and interaction properties between the particles and the buffers. Figure 6 shows in cartoon representation that nanoparticles readily form aggregates in high ionic strength solutions. This cartoon representation also shows that although these aggregates represent a great deal of the mass of nanoparticles, there is still small amount of single nanoparticles that can be detected in the solution on the order of 10 mg/L.

Dissolution of Ag nanoparticles in simulated biological fluids

The dissolution of Type I and Type II Ag nanoparticles into Ag ions in ALF and Gamble's simulated fluids was studied using ICP-OES. The bioavailability and toxicity of metal nanoparticles are often linked to the ability of the nanoparticles to deliver soluble metal ions to the specific biological organisms. Smaller particles because of their larger surface areas could deliver ions faster (Lok et al. 2007); hence, they provide greater bioavailability than larger particles. Nanosilver can be introduced to the human body in many ways, but it is unclear which form it takes when introduced to organs and other functional areas of an organism. Gamble's and ALF solutions are simulated to represent dissolution in the airway surface liquid or in the microphage phagolysosome. We did not observe any dissolution of Ag nanoparticles into Ag ions in both simulated biological fluids. Very small percentages (0.03–0.07%) of the initial Ag concentration are detected and potentially coming from a small amount of nanoparticles left in the solution after filtration and centrifugation. Since the percentages of dissolved Ag do not change after 96 h, we conclude that Ag nanoparticles do not dissolve into ions in these simulated biological fluids. Therefore, we conclude that Ag nanoparticles coexist

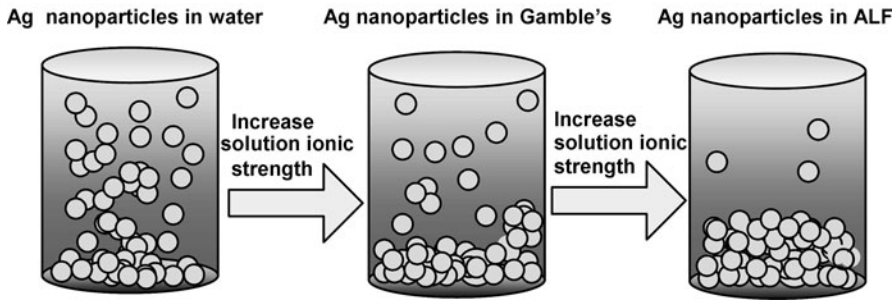

Fig. 6 Nanoparticle stability in different ionic strength solutions. This figure shows in cartoon representation that nanoparticles readily form aggregates in high ionic strength solutions. Furthermore, this cartoon representation also shows that although these aggregates represent a great deal of the mass of nanoparticles, there is some small amount of nanoparticles, which can be detected in the solution on the order of 10 mg/L

in the form of agglomerates/aggregates and dissolved single nanoparticles in these artificial biological buffers. Furthermore, we estimated that up to 1% or ca. 2–20 mg/L of Ag nanoparticles remain suspended in simulated biological fluids after 24 h and most likely exist in a single nanoparticle form which can also be observed from SMPS distributions in Gamble's solution (Figs. 2a, 3a). While the concentration of silver may vary from 0.1 to 327 ng/L in oceans and rivers (Luoma 2008), research has shown that with a concentration of only 1–5 μg/L some aquatic organisms can be killed (Wijnhoven et al. 2009). We have found that Ag nanoparticles might become bioavailable in a single nanoparticle form at these and higher concentrations. These experiments were conducted in artificial biological fluids, which simulate interstitial and lysosomal lung fluids. Due to the complexity of fluid compositions, the results are influenced by the ions present in these fluids. The results presented in this article are specific to the systems used in this study. In vivo studies would be more accurate to describe the processes which occur with Ag nanoparticles in biological systems.

Conclusions

From the results of this study, we conclude that Ag nanoparticles form aggregates and agglomerates when introduced to high ionic strength biological fluids and remain as single nanoparticles, where less than 10 mg/L of Ag nanoparticles remains suspended, and the rest forms aggregates and settle out. Ag nanoparticles precipitate faster in artificial lysosomal fluid as observed from UV–Vis spectra, due to the higher ionic strength of the buffer. Protective coatings designed to prevent nanoparticles from aggregation do not protect Ag nanoparticles against settling out in these simulated biological fluids. DLVO theory calculations support our observations that Ag nanoparticles independent of surface modification form unstable suspensions in simulated biological fluids. The release of Ag ions into interstitial or lysosomal fluids appears to be negligible as determined by ICP analysis in these simulated fluids.

Acknowledgments This article is based upon the study supported by the National Institutes of Occupational Health and Safety under Grant R01OH009448.

References

Ashrani PV, Wu WL, Gong Z, Valiyaveettil S (2008) Toxicity of silver nanoparticles in zebrafish models. Nanotechnology 19:255102

Bastus NG, Casals E, Vazquez-Campos S, Puntes V (2008) Reactivity of engineered inorganic nanoparticles and carbon nanostructures in biological media. Nanotoxicology 2(3):99–112

Borm PJA, Robbins D, Haubold S, Kuhlbusch T, Fissan H, Donaldson K, Schins R, Stone V, Kreyling W, Lademann J, Krutmann J, Warheit D, Oberdorster E (2006) The potential risks of nanomaterials: a review carried out for ECETOC. Part Fibre Toxicol 3(11):1–36

Bostrom M, Deniz V, Franks GV, Ninham BW (2006) Extended DLVO theory: electrostatic and non-electrostatic forces in oxide suspensions. Adv Colloid Interface Sci 123–126:5–15

Chen KL, Elimelech M (2006) Aggregation and deposition kinetics of fullerene (C) nanoparticles. Langmuir 22(26):10994–11001

Damm C, Münstedt H, Rösch A (2008) The antimicrobial efficacy of polyamide 6/silver-nano- and microcomposites. Mater Chem Phys 108:61–66

Darlington TK, Neigh AM, Spencer MT, Nguyen OT, Oldenburg SJ (2009) Nanoparticle characteristics affecting environmental fate and transport through soil. Environ Toxicol Chem 28(6):1191–1199

Elzey S, Grassian VH (2010) Agglomeration, isolation and dissolution of commercially manufactured silver nanoparticles in aqueous environments. J Nanopart Res 12(5): 1945–1958

Englebienne P, Hoonacker AV, Verhas M (2003) Surface plasmon resonance: principles, methods and applications in biomedical sciences. Spectroscopy (Amsterdam, Netherlands) 17(2–3):255–273

Grassian VH, O'Shaughnessy PT, Adamcakova-Dodd A, Pettibone JM, Thorne PS (2007a) Inhalation exposure study of titanium dioxide nanoparticles with a primary particle size of 2 to 5 nm. Environ Health Perspect 15(3):397–402

Grassian VH, Adamcakova-Dodd A, Pettibone JM, O'Shaughnessy PT, Thorne PS (2007b) Inflammatory response of mice to manufactured titanium dioxide nanoparticles: comparison of size effects through different exposure routes. Nanotoxicology 1(3):211–226

Guzman KAD, Finnegan MP, Banfield JF (2006) Influence of surface potential on aggregation and transport of titania nanoparticle. Environ Sci Technol 40(24):7688–7693

Heath JR (1989) Size-dependent surface-plasmon resonances of bare silver particles. Phys Rev B 40:9982–9985

Huang T, Nallathamby PD, Gillet D, Xu X-HN (2007) Design and synthesis of single-nanoparticle optical biosensors for imaging and characterization of single receptor molecules on single living cells. Anal Chem 79:7708–7718

Hussain SM, Hess KL, Gearhart JM, Geiss KT, Schlager JJ (2005) In vitro toxicity of nanoparticles in BRL 3A rat liver cells. Toxicol In Vitro 19:975–983

Ji JH, Jung JH, Kim SS, Yoon JU, Park JD, Choi BS, Chung YH, Kwon IH, Jeong J, Han BS, Shin JH, Sung JH, Song KS, Yu IJ (2007) Twenty-eight-day inhalation toxicity study of silver nanoparticles in Sprague-Dawley rats. Inhal Toxicol 19(10):857–871

Kim YS, Kim JS, Cho HS, Rha DS, Kim JM, Park JD, Choi BS, Lim R, Chang HK, Chung YH, Kwon IH, Jeong J, Han BS, Yu IJ (2008) Twenty-eight-day oral toxicity, genotoxicity, and gender-related tissue distribution of silver nanoparticles in Sprague-Dawley rats. Inhal Toxicol 20(6):575–583

Klaine SJ (2009) Considerations for research on the environmental fate and effects of nanoparticles. Environ Toxicol Chem 28(9):1787–1788

Lecoanet HF, Bottero J-Y, Wiesner MR (2004) Laboratory assessment of the mobility of nanomaterials in porous media. Environ Sci Technol 38(19):5164–5169

Lee K, Sathyagal AN, McCormick AV (1998) A closer look at an aggregation model of the Stober process. Colloids Surf A Physicochem Eng Asp 144:115–125

Lee KJ, Nallathamby PD, Browning LM, Osgood CJ, Xu X-HN (2007) In vivo imaging of transport and biocompatibility of single silver nanoparticles in early development of zebrafish embryos. ACS Nano 1:133–143

Lee K-C, Lin S-J, Lin C-H, Tsai C-S, Lu Y-J (2008) Size effect of Ag nanoparticles on surface plasmon resonance. Surf Coat Technol 202:5339–5342

Li X, Zhang J, Xu W, Jia H, Wang X, Yang B, Zhao B, Li B, Osaki Y (2003) Mercaptoacetic acid-capped silver nanoparticles colloid: formation, morphology, and SERS activity. Langmuir 19:4285–4290

Lok C-N, Ho C-M, Chen R, He Q-H, Yu W-Y, Sun H, Tam PK-H, Chiu J-F, Che C-M (2007) Silver nanoparticles: partial oxidation and antibacterial activities. J Biol Inorg Chem 12:1432–1437

Luoma SN (2008) Silver nanotechnologies and the environment: old problems or new challenges? Project on Emerging Nanotechnologies reports PEN 15

Moss OR (1979) Simulants of lung interstitial fluid. Health Phys 36:447–448

Nallathamby PD, Lee KJ, Xu X-HN (2008) Design of stable and uniform single nanoparticle photonics for in vivo dynamics imaging of nanoenvironments of zebrafish embryonic fluids. ACS Nano 2(7):1371–1380

Oberdorster G, Oberdorster E, Oberdorster J (2005) Nanotoxicology: an emerging discipline evolving from studies of ultrafine particles. Environ Health Perspect 113(7): 823–839

Pettibone JM, Elzey S, Grassian VH (2008a) An integrated approach toward understanding the environmental fate, transport, toxicity, and health hazards of nanomaterials. In: Grassian VH (ed) Nanoscience and nanotechnology: environmental and health implications. Wiley, New York, pp 43–68

Pettibone JM, Adamcakova-Dodd A, Thorne PS, O'Shaughnessy PT, Weydert JA, Grassian VH (2008b) Inflammatory response of mice following inhalation exposure to iron and copper nanoparticles. Nanotoxicology 2(4): 189–204

Pettibone JM, Cwiertny DM, Scherer M, Grassian VH (2008c) Adsorption of organic acids on TiO_2 nanoparticles. Effects of pH, nanoparticle size, and nanoparticle aggregation. Langmuir 24(13):6659–6667

Phenrat T, Saleh N, Sirk K, Kim H-J, Tilton RD, Lowry GV (2008) Stabilization of aqueous nanoscale zerovalent iron dispersions by anionic polyelectrolytes: adsorbed anionic polyelectrolyte layer properties and their effect on aggregation and sedimentation. J Nanopart Res 10:795–814

Powers KW, Brown SC, Krishna VB, Wasdo SC, Moudgil BM, Roberts SM (2006) Research strategies for safety evaluation of nanomaterials. Part VI. Characterization of nanoscale particles for toxicological evaluation. Toxicol Sci 90:296–303

SAP Minutes No. 2010-01. A set of scientific issues being considered by the Environmental Protection Agency regarding: evaluation of the hazard and exposure associated with nanosilver and other nanometal pesticide products. FIFRA Scientific Advisory Panel meeting, Environmental Protection Agency, Arlington, 3–5 Nov 2009

Scheckel KG, Luxton TP, El Badawy AM, Impellitteri CA, Tolaymat TM (2010) Synchrotron speciation of silver and zinc oxide nanoparticles aged in a kaolin suspension. Environ Sci Technol 44(4):1307–1312

Schmoll LH, Elzey S, Grassian VH, O'Shaughnessy PT (2009) Nanoparticle aerosol generation methods from bulk

powders for inhalation exposure studies. Nanotoxicology 3(4):265–275

Shah PS, Holmes JD, Johnston KP, Korgel BA (2002) Size-selective dispersion of dodecanethiol-coated nanocrystals in liquid and supercritical ethane by density tuning. J Phys Chem B 106:2545–2551

Skebo JE, Grabinski CM, Schrand AM, Schlager JJ, Hussain SM (2007) Assessment of metal nanoparticle agglomeration, uptake, and interaction using high-illuminating system. Int J Toxicol 26:135–141

Smitha SL, Nissamdeen KM, Philip D, Gopchandran KG (2008) Studies on surface plasmon resonance and photoluminescence of silver nanoparticles. Spectrochim Acta A 71:186–190

Stopford W, Turner J, Cappellini D, Brock T (2003) Bioaccessibility testing of cobalt compounds. J Environ Monit 5:675–680

Sung JH, Ji JH, Yoon JU, Kim DS, Song MY, Jeong J, Han BS, Han JH, Chung YH, Kim J, Kim TS, Chang HK, Lee EJ, Lee JH, Yu IJ (2008) Lung function changes in Sprague-Dawley rats after prolonged inhalation exposure to silver nanoparticles. Inhal Toxicol 20(6):567–574

Takenaka S, Karg E, Roth C, Schulz H, Ziesenis A, Heinzmann U, Schramel P, Heyder J (2001) Pulmonary and systemic distribution of inhaled ultrafine silver particles in rats. Environ Health Perspect 109:547–551

Vallopil SP, Pickup DM, Carroll DL, Hope CK, Pratten J, Newport RJ, Smith ME, Knowles JC (2007) Effect of silver content on the structure and antibacterial activity of silver-doped phosphate-based glasses. Antimicrob Agents Chemother 51:4453–4461

Vikesland PJ, Heathcock AM, Rebodos RL, Makus KE (2007) Particle size and aggregation effects on magnetite reactivity toward carbon tetrachloride. Environ Sci Technol 41(15):5277–5283

Wijnhoven SWP, Peijnenburg WJGM, Herberts CA, Hagens WI, Oomen AG, Heugens EHW, Roszek B, Bisschops J, Gosens I, Van De Meent D, Dekkers S, De Jong WH, van Zijverden M, Sips AJAM, Geertsma RE (2009) Nano-silver—a review of available data and knowledge gaps in human and environmental risk assessment. Nanotoxicology 3:109–138